The final publication is available at

https://doi.org/10.1039/c7nr06415b

Additional Information

Lectin-gated and glycan functionalized mesoporous silica nanocontainers for targeting cancer cells overexpressing Lewis X antigen†

R. Bhat,[a] I. García,[b] E. Aznar,[a,c,d,e] B. Arnaiz,[b] M.C. Martínez-Bisbal,[a,c,d] L.M. Liz-Marzán,[b,f] S. Penadés*[b] and R. Martínez-Máñez*[a,c,d,e]

Gated mesoporous silica nanoparticles can deliver payload upon the application of a predefined stimulus, and therefore are promising drug delivery systems. Despite their important role, relatively low emphasis has been placed on the design of gating systems that actively target carbohydrate tumor cell membrane receptors. We describe herein a new Lewis X (Le^x) antigen-targeted delivery system comprising mesoporous silica nanoparticles (MSNs) loaded with ATTO 430LS dye, functionalized with a Le^x derivative (**1**) and capped with a fucose-specific carbohydrate-binding protein (*Aleuria Aurantia* lectin (AAL)). This design takes advantage of the affinity of AAL lectin for Le^x overexpressed receptors in certain cancer cells. In the proximity of the cells, AAL is detached from MSNs to bind Le^x, and selectins in the cells bind Le^x in the gated MSN's, thereby inducing cargo delivery. Gated MSNs are nontoxic to colon cancer DLD-1 cells, and ATTO 430LS dye delivered correlated with the amount of Le^x antigen overexpressed at the DLD-1 cells surface. This is one of the few examples of MSNs using biologically relevant glycans for both capping (via interaction with AAL) and targeting (via interaction with overexpressed Le^x at the cell membrane).

Introduction

Within the wide variety of functional materials for drug delivery applications, mesoporous silica nanoparticles (MSNs) present a unique combination of features, including high stability, biocompatibility, homogeneous porosity, tunable size, large storage capacity and versatile functionalization.[1] MSNs can be functionalized to obtain gated nanoparticles, which display "zero release" unless a predefined stimulus is applied. This renders a suitable technology for the design of effective drug-delivery nanodevices.[2–12] Chemical, physical and biochemical triggers have been used to develop gated materials with controlled-release features. The use of biomolecules in capped mesoporous nanostructures has been recently demonstrated to allow for efficient drug delivery in more realistic biological settings, additionally providing selectivity in gated devices for highly specific applications.[13–21] Biomolecules can act not only as gates but also as ligands to target specific cells and tissues which display over-expressed receptors. Hence, the use of site or cell-specific delivery systems can improve therapy effectivity, the required dose can be lowered and side effects can be reduced. The targeting ability of bio-gated MSNs is usually based on surface-bound antibodies,[22] peptides [23] or aptamers.[24] However, despite their abundance and biological importance, less emphasis has been placed on a third group of relevant biomolecules, namely glycans (carbohydrates or saccharides). Cell surface glycans and glycoproteins play an important role in cell fate related to physiological and pathological processes such as cancer.[25–28] Moreover, glycosylation modifications are universal features of malignant transformation and tumor progression.[27] Glycan changes in malignant cells can occur in diverse ways, such as the lack of expression or excessive expression of certain structures, the persistence of incomplete or truncated structures, the accumulation of precursors and the appearance of novel structures.[27] Despite the great significance of this group of molecules, only simple saccharides [29–34] or the polysaccharide hyaluronic acid [35,36] have been employed in MSNs so far, to actively target carbohydrate tumor cell membrane receptors. Surprisingly, the use of glycan/protein interactions has been rarely studied in this context. To the best of our knowledge, only the interactions of Concavalin A with mannose and glucose have been used to prepare gated MSNs.[37,38] Nonetheless, in spite of their relevance, the use of multifunctional systems involving complex glycans such as the Lewis X (Le^x) antigen and lectins as targeting and gating moieties, has not yet been addressed. In particular it has been reported that the expression of such carbohydrate antigens (particularly the overexpression of sialyl-Lewis X (sLe^x)) and associated proteins (glycosidases, glycosyltransferases) changes significantly in malignant cells (aberrant glycosylation),[39–41] thereby promoting metastasis.[42] Moreover, the antigenic epitope of sLe^x carbohydrate antigen has been used clinically as a tumor marker for pancreatic cancer, colorectal cancer, bladder cancer and other malignancies.[43–45] sLe^x plays an important role in cancer cells, regarding E-selectin-mediated cell adhesion to vascular endothelial cells during the course of tumor angiogenesis and distant metastasis.[46] Furthermore, Le^x is known to be involved in selectin-mediated adhesion of cancer cells to the vascular

a. *Instituto Interuniversitario de Investigación de Reconocimiento Molecular y Desarrollo Tecnológico (IDM), Universitat Politècnica de València, Universitat de València, Camino de Vera s/n, 46022 Valencia, Spain. e-mail: rmaez@qim.upv.es*
b. *CIC biomaGUNE, and CIBER de Bioingeniería, Biomateriales y Nanomedicina (CIBER-BBN). Paseo Miramón 182, 20009 Donostia-San Sebastián, Spain. e-mail: spenades@cicbiomagune.es*
c. *CIBER de Bioingeniería, Biomateriales y Nanomedicina (CIBER-BBN), Camino de Vera s/n, 46022 Valencia, Spain.*
d. *Unidad Mixta de Investigación en Nanomedicina y Sensores Universitat Politècnica de València, IIS La Fe de Valencia, 46026 Valencia, Spain*
e. *Unidad Mixta UPV-CIPF de Investigación en Mecanismos de Enfermedades y Nanomedicina, Universitat Politècnica de València, Centro de Investigación Príncipe Felipe, Valencia, Spain.*
f. *Ikerbasque, Basque Foundation for Science, 48013 Bilbao, Spain.*
†Electronic Supplementary Information (ESI) available: PXRD patterns of as-synthesized MSNs and extracted MSNs. TEM images of MSNs and solid **S3**. N$_2$ adsorption-desorption isotherms for MSNs and pore size distribution. Release profile of ATTO 430LS dye from solid **S3** in cellular medium. See DOI: 10.1039/x0xx00000x

endothelium and is thought to be closely associated with hematogenous metastasis.[47,48] Changes in these carbohydrate-antigen expression profiles are especially remarkable in human colon cancer cells, where both sLe^x and Le^x antigens are highly expressed.[49]

With this background and inspired by such changes in cancer cells, we successfully addressed the design of a new biogated-MSN that targets and delivers cargo in tumoral cells, using a double reciprocal recognition approach. The design is based on the expression of significant amounts of i) Le^x antigen on the surface of certain cancer cells, which is recognized by fucose-binding proteins (lectins) and ii) the presence of selectins (Le^x antigen binding proteins) on the surface of cancer cells, which thus recognize the Le^x antigen. The gated system consists of MSNs loaded with a dye (ATTO 430LS), functionalized with a Le^x derivative (1) and capped with a fucose-specific carbohydrate-binding protein (*Aleuria Aurantia* lectin (AAL)). Gated nanoparticles were tested in PBS buffer and in the DLD-1 human colorectal adenocarcinoma cell line, with high expression of sLe^x and Le^x antigen-binding sites. AAL-gated MSNs did not show toxicity toward colon cancer DLD-1 cells, whereas ATTO 430LS dye delivery was found to be

Table 1. Mean hydrodynamic diameter obtained from DLS studies of MSN and solids S1, S2 and S3.

| MSN (nm)	S1 (nm)	S2 (nm)	S3(nm)
202	243	255	260

dependent on the amount of Le^x antigen overexpressed on the DLD-1 cells surface.

Results and discussion

Design and synthesis of lectin-capped MSNs
The design of the controlled-release nanomaterial is depicted in Fig. 1a. MSNs were loaded with the ATTO 430LS dye and surface-functionalized with the fucose-containing Le^x (Galβ1-4[Fucα1-3]GlcNAcβ-1) antigen derivative **1** (**S2** in Fig. 1a).

As capping system, the fucose-specific carbohydrate-binding protein AAL was selected. AAL was expected to interact with the Le^x antigen via multivalent fucose-lectin
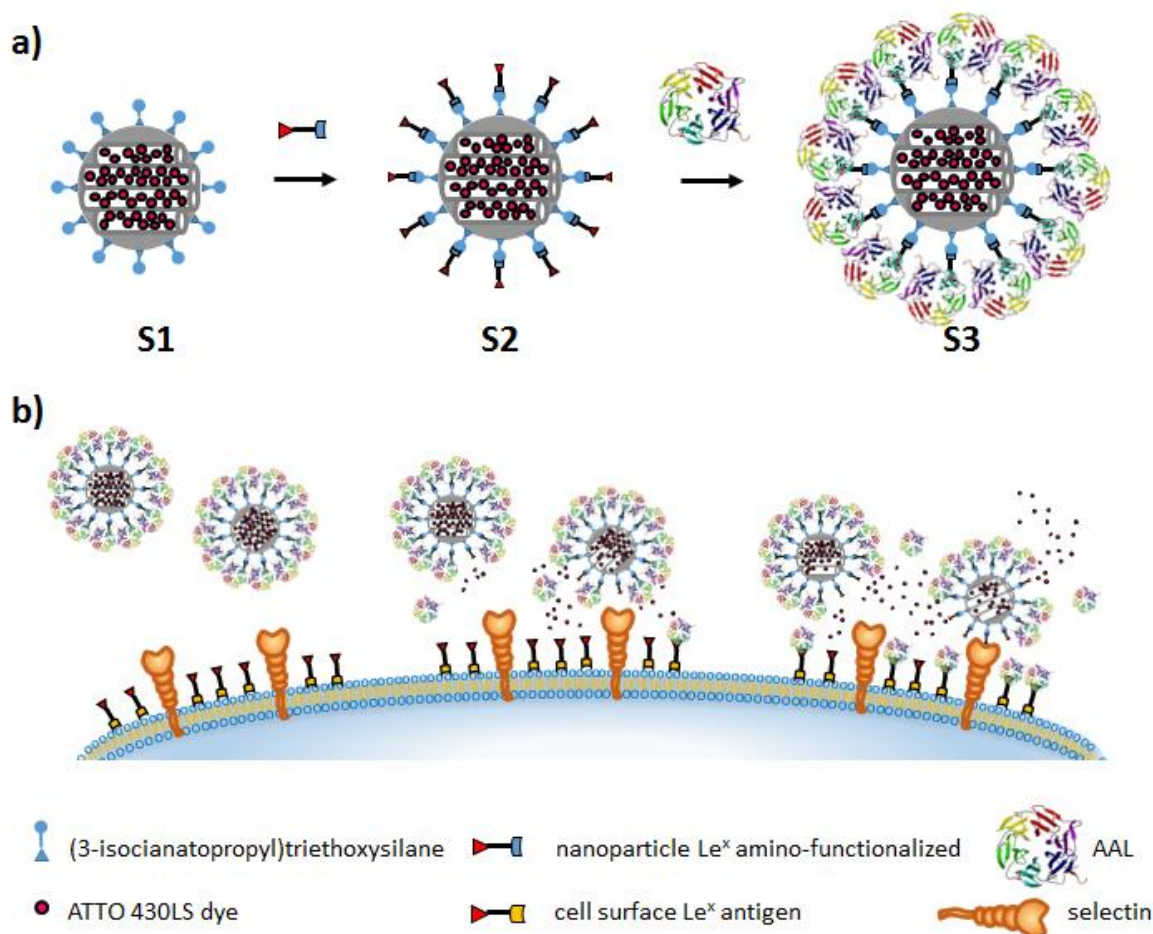
Fig. 1 a) Representation of the solids synthetized to obtain the lectin-gated and Le^x antigen-functionalized MSNs (S3). b) Opening of the gated system in the presence of specific cellular receptors and cargo release. AAL is detached from MSNs to bind Le^x at the cell membrane, and selectins in the cells bind Le^x in the gated MSNs, thereby favoring internalization and inducing cargo delivery.

interactions, thereby inhibiting cargo release (**S3** in Fig. 1a). The opening of gated MSNs would be based on a displacement reaction via AAL binding onto overexpressed Le[x] receptors, at the cell membrane. Moreover, the anchored Le[x] antigen derivative **1** on the MSNs was expected to additionally bind fucose-binding proteins (selectins) on the cell surface, favoring endocytosis of the nanoparticles (Fig. 1b). Therefore, the Le[x] antigen plays a double role: on one hand as a linking molecule to AAL, so that the pores are capped, and on the other hand as targeting agent toward selectins. At the same time, the AAL lectin also plays a double role: capping the pores via interaction with Le[x] derivative **1**, and targeting overexpressed Le[x] receptors on the cell membrane (see Fig. 1).

In the present work, MCM-41-based MSNs were selected.[50] The mesoporous nanoparticles were prepared by using precursor and the surfactant hexadecyl-trimethylammonium bromide (CTABr) as the porogen species. Bare MSNs were obtained upon surfactant removal by extraction. The inorganic support was then loaded with the fluorescent dye ATTO 430LS, and the outer surface of the nanoparticles was functionalized with (3-isocyanatopropyl)triethoxysilane to obtain solid **S1** (Fig. 1a). Reaction of the isocyanate groups with the amino-functionalized Le[x] antigen derivative **1** yielded solid **S2**. Finally, the nanoparticles were capped in PBS, in the presence of AAL (solid **S3**). Cargo delivery from **S3** was anticipated to occur only in the presence of increased amounts of fucose or fucose-containing glycans. Buffered suspensions of solid **S3** can be stored at 4º C during weeks without any loss of functionality.

The amino-functionalized Le[x] antigen derivative **1** was obtained by following established protocols,[51] with two main modifications (Fig. 2). For the synthesis of the trisaccharide Le[x], 3,4,6-tri-O-acetyl-2-deoxy-2-(2,2,2-trichloroethoxycarbonylamino)-1-(2-N-Benzyloxycarbonylaminoethyl)-D-glucopyranoside (1) pertrimethylsilyl-L-fucose (2) and 2,3,4,6-Tetra-O-acetyl-D-galactopyranose (3), were prepared as monosaccharides building blocks for the Le[x] synthesis (Fig. 2). First, a trichloroethyloxycarbonyl (Troc) was employed as amino protecting group, which ensures high glycosyl accepting properties of the C-3 hydroxyl of the glucosamine unit [52] and

offers efficient neighboring group participation to yield stereoselective formation of β-glycoside. The trisaccharide Le[x] was chemically synthesized bearing an amino-ended linker for attaching to the mesoporous surface using thiourea linkage.[53]

Materials characterization

MSNs and solids **S1**, **S2** and **S3** were characterized by standard techniques. Powder X-ray diffraction (PXRD) of as-made MSNs (see Fig. S1 in ESI†) showed four low-angle peaks, corresponding to the (100), (110), (200) and (210) reflections of a hexagonal array, typical of MCM-41-type mesoporous materials. After extraction of the surfactant template, a slight shift of the main peak (assigned to the (100) Brag reflection) was observed, corresponding to a cell contraction of ca. 2 Å (see Fig. S1 in ESI†). From N_2 adsorption-desorption isotherm studies, a typical curve for mesoporous materials was observed for calcined MSNs. Application of the BET model yielded a total specific surface of 955.2 m^2/g and a pore volume of 0.75cm^3/g. The BJH model was also used at intermediate relative pressures, resulting in a narrow pore distribution centered at 2.52 nm (see Fig. S5 in ESI†). A cell parameter a_0 of 4.35 nm and wall thickness of 1.83 nm were calculated. Nanoparticles **S1**, **S2** and **S3** were obtained in relatively low amounts and could not be characterized by ~~PXRD and~~ N_2 isotherm studies~~.~~

All materials were characterized by Transmission Electron Microscopy (TEM). The presence of spherical mesoporous nanoparticles with a diameter of *ca.* 200 nm was clearly observed in all samples (see Fig. S3 in ESI†). Dynamic light scattering (DLS) was used to assess the hydrodynamic diameter of the particles. Table 1 summarizes the obtained data for the starting MSNs, **S1**, **S2**, and **S3**. A gradual diameter increase was observed from bare nanoparticles (202 nm) to solid **S2** (255 nm) and from solid **S2** to **S3** (260 nm). Finally, the organic content of **S1**, **S2** and **S3** was determined by thermogravimetric and elemental analysis (TGA). Table 2 shows the organic content of ATTO 430LS dye, 3-isocyanatopropyl, Le[x] antigen derivative and AAL in %wt.

Delivery studies in solution

Troc = 2,2,2-trichloroethoxycarbonyl
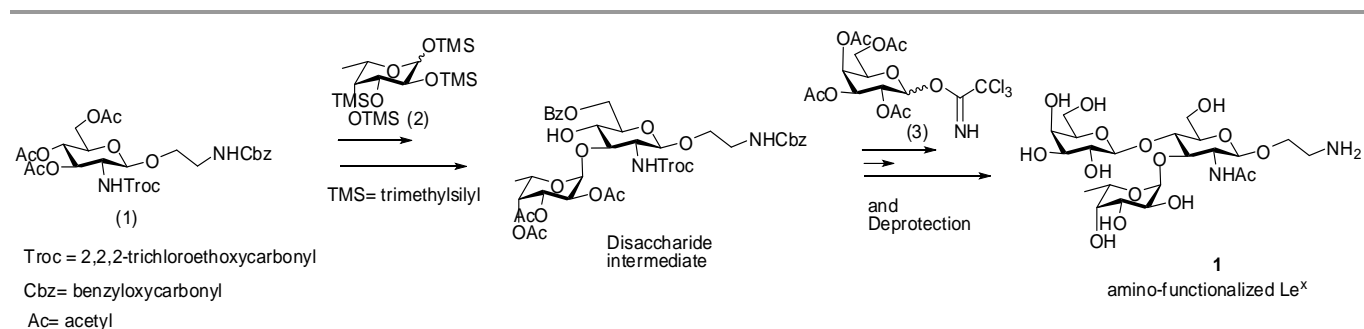
Cbz= benzyloxycarbonyl

Ac= acetyl

Fig. 2 Synthesis of Le[x] antigen derivative **1**.

Retaining cargo inside a carrier until the target is reached is a crucial requirement in drug delivery systems, so as to reduce side effects and increase drug efficacy. Cargo release studies of **S3** where therefore carried out, taking advantage of the high affinity of AAL for L-fucose. In a typical experiment, **S3** was suspended in water and the suspension was fractionated into two parts. To one fraction L-fucose was added. Both suspensions were stirred and aliquots were taken at the scheduled times. After centrifugation to remove the solid, the fluorescence of the ATTO 430LS dye delivered to the solution was measured at 547 nm (λ_{ex} = 433 nm). The drug delivery profile for both experiments is displayed in Fig. 3.

In the absence of L-fucose, a flat baseline was obtained, which indicates that ATTO 430LS remained in the pore voids of the nanoparticles, not being released during the time of the experiment. In particular, cargo delivery was lower than 10% after 1 h. In contrast, in the presence of L-fucose, ATTO 430LS release was indicated by an increase in fluorescence with time. The observed behavior is in agreement with a displacement reaction, in which AAL binds L-fucose, the pores are uncapped and payload delivered. To assess the performance of **S3** in competitive media, delivery experiments were carried out in cell culture medium, in the presence and in the absence of L-fucose, with similar results (see Fig. S9 in ESI†).

Evaluation of MSNs S3 in colon cancer cells with high expression of Le[x] antigen

Controlling cell targeting and penetrability of drugs is a major issue in nanomedicine. Therefore, after demonstrating the effective capping and cargo release of **S3**, we evaluated the ability of **S3** nanoparticles to target human colorectal adenocarcinoma DLD-1 cells. [34] In a first step, the presence of AAL-binding ligands (Le[x]) on DLD-1 cells was confirmed using labelled AAL (i.e. AAL555). Fluorescence images of cells treated with AAL555 (Fig. 4a) showed a clear membrane staining pattern (red), which was not found in control DLD-1 cells

**Table 2** Organic content in wt% for solids **S1**, **S2** and **S3**.

	ATTO 430LS dye	3-isocyanatopropyl	Le[x] antigen derivative	AAL
S1	3.50	2.77	---	---
S2	3.26	2.59	6.08	---
S3	3.11	2.47	5.80	3.89

treated only with media (Fig. 4b). These results corroborated the expression of AAL-binding ligands (i.e. Le[x]) on the DLD-1 membrane. In a second step, the effect of **S3** on DLD-1 cell viability was studied. DLD-1 cells were treated with different concentrations of **S3** for 24 h and cell viability was determined by MTS assays. [54,55] Results are shown in Fig. 5a, in which values are given as a mean of quadruplets ± S.D. The AAL-gated solid **S3** did not affect the viability of DLD-1 cells after 24 h incubation at concentrations up to 10 µg/mL.

Internalization of **S3** on DLD-1 cells and dye delivery were also studied. Experiments were carried out in duplicates. Fluorescence microscopy experiments on DLD-1 cells after 4 h incubation with **S3** showed the release of ATTO 430LS inside the cells (Fig. 5b). Interestingly, cells incubated with **S3** for 24 h showed a brighter green staining (Fig. 5c, 5d), in agreement with a higher amount of ATTO 430LS released with time. Confirmation of cargo release induced by the selective uncapping of **S3** – due to AAL displacement to bind the Le[x] ligands present on DLD-1 membrane – was carried out via similar experiments using DLD-1 cells in which Le[x] and sLe[x] expression was induced. Overexpression of Le[x] (and sLe[x]) was prompted by culturing cells in the presence of epidermal growth factor (EGF) and basic fibroblast growth factor (bFGF). [56] From the analyses of these cultures by flow cytometry, it was concluded that the highest expression of Le[x] and sLe[x] was achieved when DLD-1 cells were cultured for 3 days in the presence of EGF and bFGF (see Fig. 6).
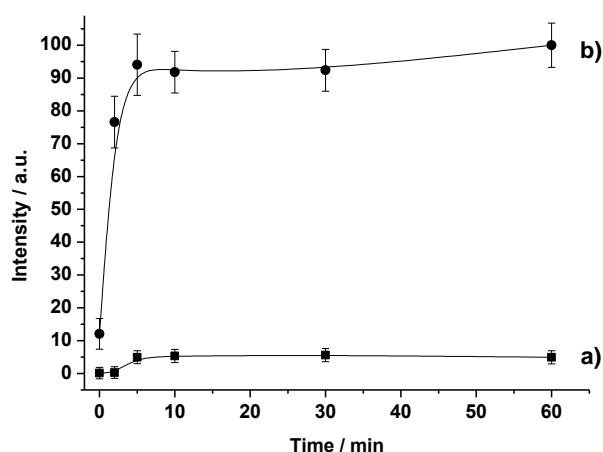
Fig. 3 Release profile of ATTO 430LS dye from solid **S3** in the absence (a) and in the presence (b) of L-fucose
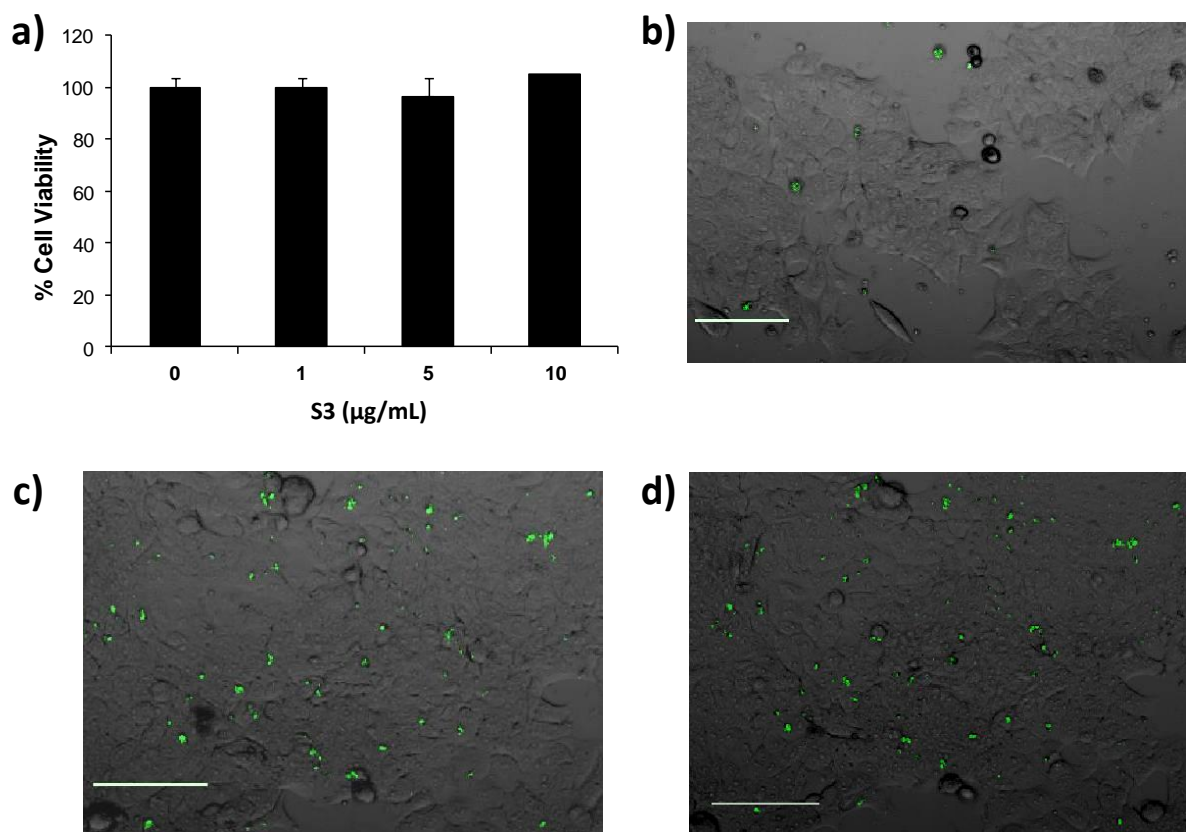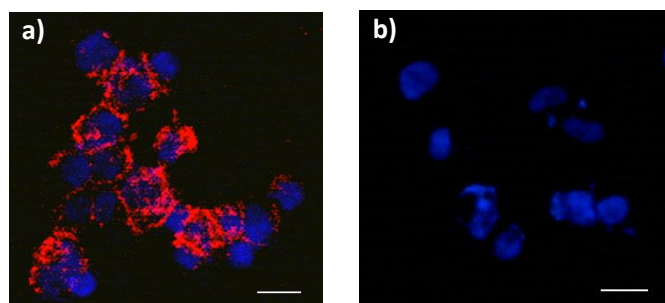
Fig. 5 a) S3-DLD-1 viability assay with the colorimetric MTS method. Experiments were carried out in quadruplets and data are plotted as mean ± SD. b-d) S3-cell interaction assessment. Confocal microscopy imaging of DLD-1 cells after incubation with S3 for 4h (b), 24h (c,d), not washed (b,c) and washed with PBS (d). The same region was considered for images c) and d). Experiments were carried out in duplicates. 10x magnification. Scale bar: 100 μm.

Le^x and sLe^x-overexpressing DLD-1 cells and untreated DLD-1 cells were incubated with solid **S3** for 24 h. Experiments were carried out in duplicates. Fluorescence images showed a higher ATTO 430LS emission in cells treated with EGF and bFGF (Fig. 7a) than in control cells (Fig. 7b). Green pixels in fluorescence images were counted using the image processing program Image J, and a 3 fold higher ATTO 430LS emission was found in overexpressed Le^x cells. This increase in fluorescence correlates well with the increase of Le^x on DLD-1 cells.

Fig. 4 Fluorescent microscopy images of DLD-1 cells incubated with media with 40 μg/mL AAL555 (red) (a) or only media (b). Nuclei were stained with DAPI (blue). Magnification: 10x. Scale bar: 30 μm.

Colocalization studies performed with overexpressed Le^x and sLe^x DLD-1 cells and **S3** were also carried out. Experiments

were carried out in duplicates. Most ATTO 430LS dye (green) was found to be internalized and only a small fraction was localized with the plasma membrane (yellow) (Fig. 8a). The orthogonal view of the Z stack (Fig. 8b) confirmed that both ATTO 430LS and nuclei (DAPI-stained, blue) were present at the same planes in the cytoplasm, confirming successful internalization of the gated nanoparticles **S3**.
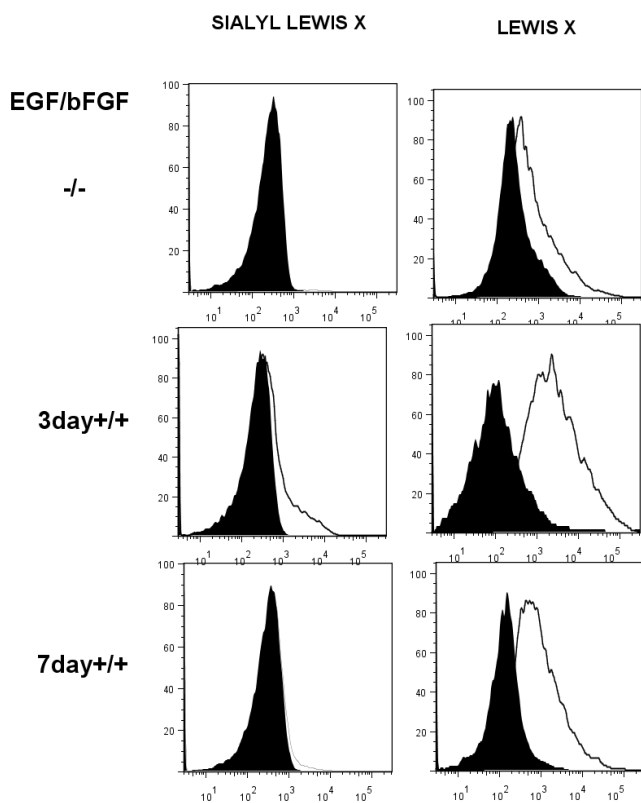
Conclusions

In summary, we have developed gated Le^x-targeted delivery systems (**S3**), using MSNs functionalized with a Le^x derivative and capped with AAL. Le^x in solid **S3** acts as an ideal linker to promote the positioning of AAL onto the surface of the nanoparticle and subsequent pore blockage. In this nanosystem, AAL was able to cap the pores in MSNs and to block cargo release (the ATTO 430LS dye). The gated solid displayed a poor cargo delivery, whereas the presence of L-fucose readily induced pore opening and payload delivery. The observed behavior is in agreement with a displacement reaction in which AAL binds L-fucose, the pores are uncapped and payload delivered. Cell viability studies showed that the gated solid **S3,** at concentrations up to 10 μg/mL, did not affect the viability of DLD-1 cells after 24 h incubation. Cargo release in cells was induced by selective uncapping of **S3** deriving from the displacement of AAL, to bind Le^x and sLe^x ligands present in

Fig. 6 Expression of Le^x and sLe^x on DLD-1 cells. DLD-1 cells were cultured for 3 or 7 days, in the presence or in the absence of EGF and bFGF. Data from PE-labelled anti-CD15 (Le^x) mAb and BD Horizon™ BV711-labelled anti CD15S (sLe^x) are shown in empty histograms. Filled histograms show isotype fluorescently labeled control antibodies, used as negative controls.

the cell membrane. In a second step, when the particles are in the proximity of cancer cells, and AAL is detached from **S3** to bind Le^x overexpressed in certain cancer cells, Le^x in the gated MSNs act as targeting agent which helps to the nanoparticle's internalization assisted by its recognition by selectins. Then, once uncapped, the anchored Le^x-derivative on MSNs would additionally bring the nanoparticle close to the membrane, by interaction with fucose-binding proteins on the cell surface (selectins). This dual targeting facilitates the specific release of cargo in tumoral cells, and helps the whole system to be internalized. Uncaping of **S3** and cargo delivery was demonstrated to occur in DLD-1 cells, whilst enhanced internalization was observed in DLD-1 cells, in which Le^x expression was enhanced. These results can be considered as promising towards adopting new therapeutic strategies to kill

malignant cancer cells that overexpress Le^x and sLe^x, which play important roles in tumor metastasis and angiogenesis. This is one of the few examples based in MSNs that use "saccharides" for capping (via interaction with AAL) and targeting (via interaction with Le^x expressed on membranes). We propose that our synthetic strategy can contribute to further design improved delivery systems using highly specific saccharides, such as Le^x, which play crucial roles in tumor angiogenesis and metastasis.

Methods

Chemicals

Tetramethylorthosilicate (TMOS), n-cetyltrimethylammonium bromide (CTAB), sodium hydroxide (NaOH), and (3-isocyanatopropyl)triethoxysilane, triethylamine, as well as all chemicals and solvents for Le^x antigen derivative synthesis, were purchased from Sigma-Aldrich. Methanol, ethanol, hydrochloric acid (HCl) and acetonitrile were purchased from Scharlab. The dye ATTO 430LS was purchased from ATTO-TECH GmbH. Silica gel (0.041-0.0631) for flash column chromatography was purchased from Merck. AAL, AAL555, L-fucose and DAPI-containing hardening mounting oil, were purchased from Vector Labs. Sodium pyruvate, Glucose, Hepes, Glutamine, Paraformaldehyde, NaAz were purchased from Invitrogen. CDCl$_3$ and TMS for NMR experiments were provided by Euriso-top (France). The human colorectal adenocarcinoma cell line (DLD-1) was purchased from American Type Culture Collection (ATTC). 3[4,5-Dimethylthiazol-2-yl]-5-(3-carboxymethoxyphenyl)-2-(4-sulfophenyl)2H-tetrazolium, inner salt (MTS) and phenazine ethosulfate (PES) were provided by CellTiter. Aqueous One Solution Cell Proliferation was purchased from Promega, UK. Cell dissociation solution, cell culture RPMI-1640 medium and streptomycin/penicillin solution were provided by Sigma. Fetal bovine serum (FBS) and fetal calf serum were provided by Lonza. EGF and HBBS (without Ca or Mg) were provided by Gibco. bFGF was purchased from Invitrogen. All chemicals were of reagent grade and used without further purification. Solvents were dried by standard procedures and reactions requiring anhydrous conditions were performed under nitrogen atmosphere. Thin layer chromatography was carried out on 0.25 mm pre-coated silica gel plates (Merck silica hgel 60 F254) with detection by UV-light (254 nm) and/or heating with 10% sulfuric acid (aqueous solution) or p-anisaldehyde solution. Flash chromatography was carried out using the SP1 Flash Purification System by Biotage.

Techniques
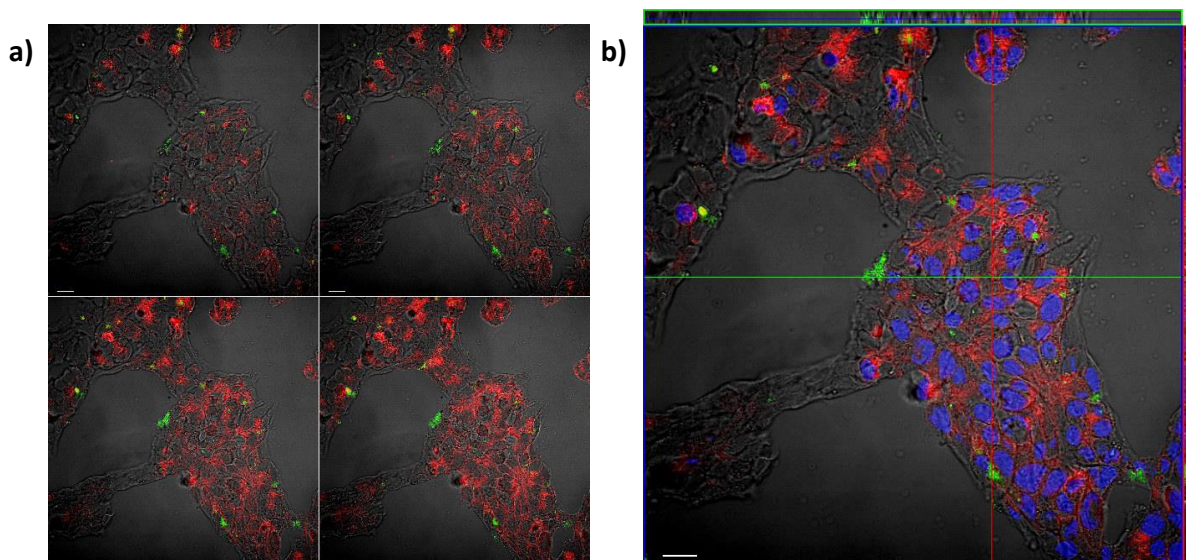
Fig. 8 Colocalization study of **S3** and DLD-1 cells plasma membrane. Cells were cultured for 3 days, in the presence of growth factors and incubated for 24 h with 8 µg/mL of the gated solid **S3** (ATTO 430LS, green), and stained for plasma membrane (red) and nuclei (blue). Z-stack images of 2 µm sections were obtained with a 40x oil objective. **a)** Gallery view, **b)** Ortho view. Scale: 20 µm. Experiments were carried out in duplicates.

PXRD, TEM, isothermal N$_2$ adsorption-desorption, DLS, FTIR spectroscopy and TGA were used to characterize the syntethized materials. PXRD measurements were performed on a Bruker AXS D8 Advance diffractometer using Cu-K$_\alpha$ radiation. TEM images were acquired with a JEOL TEM-1010 electron microscope working at 100 kV. N$_2$ adsorption-desorption isotherms were recorded on a Micromeritics TriStar II sorption analyzer. The samples were degassed at 120 °C under vacuum overnight. The specific surface areas were calculated from adsorption data within the low pressure range, using the BET model. Pore size was determined by the BJH method. DLS measurements were performed on a ZetaSizer Nano instrument from Malvern. FTIR spectroscopy was carried out with a Tensor 27 FT-IR spectrometer from Bruker. TGA was carried out on a TGA/SDTA 851e Mettler Toledo, using oxidant atmosphere (air, 80 mL/min), with a heating program consisting on a heating ramp of 10 °C per minute from 393 K to 1273 K and an isothermal heating step at this temperature for 30 minutes. Fluorescence measurements were carried out in a JASCO FP-8500 Spectrophotometer. ^{1}H-NMR spectra were run in CDCl$_3$ at 300 K on a Bruker AVANCE 400 MHz using TMS as internal reference for chemical shifts. Mass spectra were obtained with an ESI apparatus Bruker Esquire 3000 plus.

Synthesis of MSNs

MSNs were synthesized using CTAB as porogen species and TMOS as a silicon source. In brief, 3.94 g of CTAB was dissolved in a solution containing 800 g of methanol/water (0.4/0.6=w/w) and 2.8 mL of an aqueous solution of NaOH 1M, under vigorous stirring. Once dissolved, 1.3 mL of TMOS was added at ambient conditions. After being stirred for 8h, the mixture was aged overnight at rest. The resulting white precipitate was washed with ethanol and water for five times each and finally dried at 70 ºC to obtain the as-made mesostructured nanoparticles. Hence, the obtained solid was suspended in a solution containing 20 mL of ethanol and 4 mL of HCl. The suspension was refluxed overnight to extract the

surfactant template. The resulting white solid was filtered out and thoroughly washed with ethanol and water and dried under vacuum to obtain the MSNs.
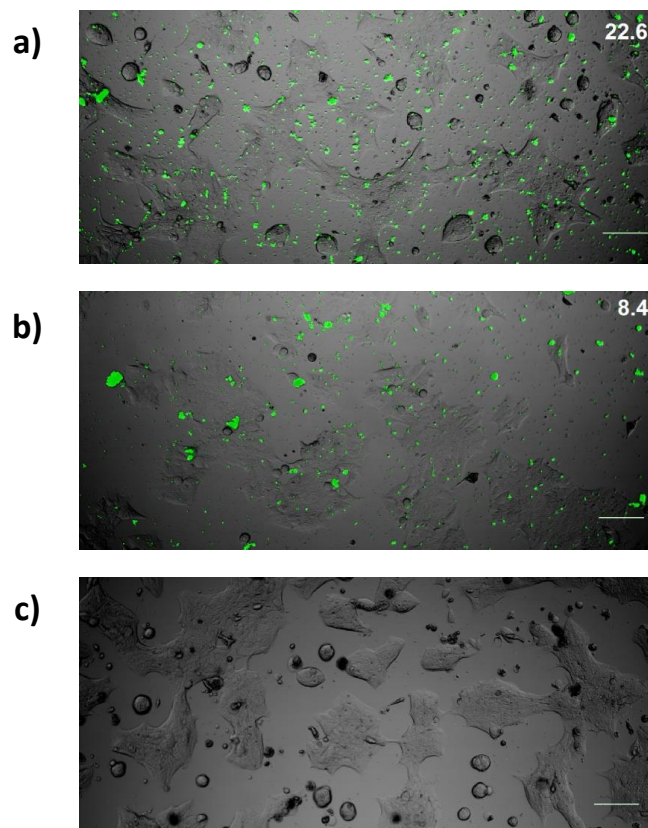
Fig. 7 DLD-1 cultured for 3 days in the presence (a) or in the absence (b,c) of growth factors, and incubated with 8 µg/mL of solid **S3** (a,b) or only media (c), for 24 h. Scale bar: 100 µm. The green color pixel percentage is shown in the top right corner. Experiments were carried out in duplicates.

Synthesis of the trisaccharide Le^x derivative (1)

Le^x derivative was obtained following the established procedure described in the literature [51,52] and in Fig. 2. A step-wise glycosylation strategy of the adequate building blocks was used. The attachment of the fucosyl residue to the 3-hydroxy group of the glucosamine moiety was followed by introduction of the galactosyl residue to the 4-hydroxyl group of the disaccharide obtained in the first glycosidation. The obtained trisaccharide was deprotected, purified and characterized by ^{1}H-NMR and mass spectrometry. ^{1}H-NMR (500 MHz, D$_2$O, 300 K): δ 1.16 ppm (d, 3H, J = 6.6 Hz, CH$_3$ Fuc), 2.02 ppm (s, 3H, OCOCH$_3$), 2.94 ppm (m, 2H, -CH$_2$-NH$_2$), 3.51 ppm (dd, 1H, J =7.4, 3.9 Hz), 3.61 ppm (m, 2H), 3.78-3.64 ppm (m, 5H), 3.80 ppm (d, 1H, J= 2.4 Hz), 3.98-3.84 ppm (m, 7H), 4.02 ppm (m, 1H), 4.44 ppm (d, 1H, J= 7.8 Hz, H1"Gal), 4.55 (d, 1H, J= 7.8 Hz, H1' Glc), 4.82 ppm (m, 1H, H5 Fuc), 5.10 ppm (d, 1H, J= 3.9 Hz, H1 Fuc) (see the complete assignment and the NMR spectra in ESI†, Fig. S6, S7 and S8, and Tables S1 and S2). Mass spectrometry data identified the following ions with m/z ratio of 573.55 (M+H)$^+$ and 287.28 (M+2H)$^{2+}$.

Synthesis of S1

50 mg of MSNs was suspended in 500 µL of an aqueous solution of ATTO 430LS dye (500 µg). The suspension was kept under stirring at room temperature overnight, to achieve maximum loading in the pores of the MSN scaffolding. Then, the solid was filtered and dried under vacuum. Subsequently, 30 mg of the dry solid was suspended in 900 µL of acetonitrile and 8 µL of (3-isocyanatopropyl)triethoxysilane was added. The mixture was stirred at room temperature for 5.5 h. Finally, the solid was filtered and dried under vacuum to obtain the solid **S1** (Fig. 1a).

Synthesis of S2

25 mg of the isocyanate-functionalized nanoparticles **S1** and 2 mg of the Le^x derivative **1** were suspended in 1 mL of deionized water. Immediately, 1 µL of triethylamine (0.003 mmol) was added as catalyst and the suspension was stirred for 2 hours. The nanoparticles were then centrifuged and washed, and the resulting Le^x-derivatized nanoparticles **S2** were finally dried under vacuum (Fig. 1a).

Synthesis of S3

1000 µg of solid **S2** was suspended in 980 µL of PBS buffer (10 mM, pH 7.4, supplemented with calcium chloride 1 mM and magnesium chloride 2 mM) and then, 20 µL of AAL aqueous solution (1.241 µg/µL) was added. The suspension was kept stirring for 1 hour at room temperature. After that time, the solid was centrifuged, washed 5 times with buffer solution and dried under vacuum to obtain the final AAL-gated solid **S3** (Fig. 1a).

Delivery studies in solution

Delivery studies of ATTO 430LS dye were performed in solution with **S3**, in the presence and in the absence of L-fucose. In a typical experiment, 500 µg of **S3** was suspended in 1000 µL of deionized water. Then, 490 µL of the suspension was mixed with 510 µL of PBS buffer (10 mM, pH 7.4) and used as a control. 490 µL of the same suspension was mixed with 510 µL of a solution of L-fucose (5 M) in PBS buffer. In both cases, the suspensions were stirred at room temperature and aliquots (130 µL) were taken at scheduled times (0, 2, 5, 10, 30, and 60 min, respectively). The aliquots were then centrifuged to remove the solid and the amount of ATTO 430LS dye delivered was measured by fluorescence spectroscopy (λ_{ex}: 433 nm, λ_{em}: 547 nm). To assess the performance in competitive media, delivery experiments were also carried out in cellular medium in the presence and in the absence of L-fucose. Solid **S3** (0.25 mg/mL) was incubated for 24 h at room temperature, in the presence and in the absence of L-fucose 2.5 M in DLD-1 complete media. The amount of delivered ATTO 430LS dye in the supernatant solution was measured by fluorescence spectroscopy (λ_{ex}: 433 nm, λ_{em}: 547 nm).

Experiments with cells

The human colorectal adenocarcinoma cell line DLD-1 was grown in RPMI-1640 medium supplemented with 10% fetal calf serum, 1 mM sodium piruvate, 4.5 g/L glucose, 10 mM HEPES, 2 mM L-glutamine and streptomycin/penicillin (100 U/mL penicillin and 100 µg/mL streptomycin) solution. Cells were cultured at 37 ºC and 5% CO$_2$ in 25 cc TC flasks. Fluorescence microscopy was used to assess the presence of AAL-binding ligands on DLD-1 plasma membrane and to test the interaction with AAL. Round coverslips (13 mm-diameter) were deposited into 24-well plates and 2x10^5 DLD-1 cells were seeded in each well. Following overnight culture, the cell monolayers were rinsed with PBS and media containing 40 µg/mL fluorescent AAL (AAL555) or media alone was added to the wells. Following a 2 h incubation at 37 ºC and 5% CO$_2$, cells were washed carefully, not to lift cells off the coverslip, and fixed with PBS containing 1% paraformaldehyde for 30 min at 37 ºC. The wells were then washed extensively and the cover slips mounted with DAPI-containing hardening mounting oil. Following a 30 min-incubation of the slides at 4 ºC the cells were imaged using the 10x magnification objective of a Leica DMI6000b microscope (λ_{ex} 560/40 nm, 595nm dichromatic mirror, λ_{em} 645/75 nm) with a Leica DFC300FX color camera.

Cell viability experiments

Cell viability was measured with the colorimetric MTS method. The MTS assay is based on the conversion of a tetrazolium salt into a colored, aqueous soluble formazan product by mitochondrial activity of viable cells at 37 °C. The amount of formazan produced by dehydrogenase enzymes is directly proportional to the number of living cells in culture and can be measured at 492 nm. [54,55] 10^4 DLD-1 cells were seeded in 96-well plates and grown for 24 h at 37 ºC and 5% CO$_2$. DLD-1 cells were incubated with media containing 1, 5 or 10 µg/mL of solid **S3** (50 µL) or media alone for 24 h at 37 ºC and 5% CO$_2$. Experiments were carried out in quadruplets. 1 h prior to absorbance measurement, the media was replaced by fresh media containing 1:20 (v:v) 3[4,5-Dimethylthiazol-2-yl]-5-(3-carboxymethoxyphenyl)-2-(4-sulfophenyl)2H-tetrazolium, inner salt (MTS) and phenazine ethosulfate (PES) and incubated at 37 ºC and 5% CO$_2$. Absorbance of MTS product was detected in a microplate reader (GENios Pro, TECAN) at 492 nm. The concentration of **S3** in PBS employed for the cell assays was determined by Inductively Coupled Plasma Optical Emission Spectroscopy.

S3-cell interaction experiments

Confocal microscopy was used to assess **S3**-cell interaction. A Zeiss LSM 510 META confocal microscope was employed. DLD-1 cells were seeded in equal numbers per well and grown for 3 days in 16-well chamberslides (Lab Tek). After removal of the culture media, DLD-1 cells were incubated with **S3** (2.7 µg/mL) in media for 4 h or 24 h at 37 ºC and 5% CO_2. Then the cell monolayers were or not washed with PBS for live cell imaging. Experiments were carried out in duplicates. The sample was excited at 488 nm and the emission light collected from 520-700 nm. The chamberslide was examined under the confocal microscope with a 10x objective in channel mode at the excitation wavelength of 488 nm for ATTO 430LS dye. The green color pixels were counted using the image analysis software Image J and the ratio to the total pixels was calculated.

Overexpression of Le[x] (and sLe[x])

DLD-1 cell surface expression of the fucose-containing carbohydrate structures Le[x] and sLe[x] was tested by flow cytometry. DLD-1 cells were grown for 3 or 7 days in the presence or absence of EGF (20 ng/mL) and bFGF (10 ng/mL). Cell monolayers were lifted from the flask surface by 15 min incubation at 37 ºC with cell dissociation solution (Sigma) and centrifuged at 1500g for 5 min. The cell pellet was re-suspended in 1% FBS, 0.09% NaAz (staining buffer) containing additional 10% of heat inactivated FBS, syringe-disaggregated and left at room temperature for 30 min to block Fc receptors. Then, 20 µL of phycoerythrin (PE)-labelled anti-human Le[x] (CD15, clone HI98) or 10 µL BD Horizon™ BV711 anti-human sLe[x] antibodies (CD15S, clone CSLEX1) were added and incubated in ice for 30 min. As control, isotype-matched fluorophore-matched antibodies were used (BD biosciences). Before analysis, cells were washed twice with staining buffer by centrifugation, re-suspended in HBBS without calcium or magnesium containing 10 µg/mL DAPI and placed in ice. As DAPI is an exclusion dye, only cells negative for DAPI staining (live cells) were analyzed. Cell doublets were also excluded from the analysis. Experiments were acquired in a BD Canto II flow cytometer (Becton Dickinson) keeping the same voltage settings for all the parameters analyzed. Analysis of the data was performed with the FlowJo program (Miltenyibiotec).

Colocalization studies

DLD-1 cells were grown for 3 days in 16-well chamber slides (Lab Tek) in the presence or absence of growth factors, then incubated with **S3** (8 µg/mL) in media for 24 h at 37 ºC and 5% CO_2 and cooled for 30 min at 4 ºC. The cell-containing wells were washed twice very carefully, drop-wise, to avoid lifting cells off the glass with cold PBS without calcium or magnesium containing 0.09% sodium azide (PBS/NaAz) and incubated with 30 µg/mL FM-464 in PBS/NaAz for 1 min at 4 ºC for membrane staining. Medium was removed and cells were fixed by incubation at 4 ºC with 4% paraformaldehyde-containing PBS/NaAz for 30 min. Then the chamber gasket was removed from the slide and the cells were rinsed twice with PBS. Experiments were carried out in duplicates. A drop of DAPI-containing mounting oil was added to each cell spot and the slide was mounted with a coverslip of 0.13-0.16 mm (25 x 60 mm, Menzel-Glazer). The oil in the mounted slide was allowed to harden by a 30 min incubation at 4 ºC, and the slide was examined under the Zeiss LSM 510 META confocal microscope with a 40x oil immersion objective in a lambda or channel mode at the excitation wavelengths of 488 nm and 514 nm for ATTO 430LS dye and FM4-64 (Life Technologies), respectively. Z-stacks of 2 µm-thickness planes were taken under the described conditions. Linear unmixing of the overlapping two spectra was performed and the resulting imaged was overlayed with the image of the transmitted light channel and the DAPI stain channel (excitation at 405 nm / emission filter 420-480 nm). For the overlays the AxioVision image program was employed.

Conflicts of interest

There are no conflicts to declare.

Acknowledgements

Notes and references

1   C. Argyo, V. Weiss, C. Bräuchle and T. Bein, *Chem. Mater.*, 2014, **26**, 435–451.

2   E. Aznar, R. Martínez-Máñez and F. Sancenón, *Expert Opin. Drug Deliv.*, 2009, **6**, 643–655.

3   E. Aznar, M. Oroval, L. Pascual, J. R. Murguía, R. Martínez-Máñez and F. Sancenón, *Chem. Rev.*, 2016, **116**, 561–718.

4   X. Wang, L.-L. Tan, X. Li, N. Song, Z. Li, J.-N. Hu, Y.-M. Cheng, Y. Wang, Y.-W. Yang, Y.-W. Yang, N. A. Kotov, L. M. Liz-Marzán, H. Mattoussi, P. Mulvaney, C. B. Murray, A. L. Rogach, P. S. Weiss, I. Willner and W. J. Parak, *Chem. Commun.*, 2016, **52**, 13775–13778.

5   X. Chen, H. Sun, J. Hu, X. Han, H. Liu and Y. Hu, *Colloids Surfaces B Biointerfaces*, 2017, **152**, 77–84.

6   R. Prasad, S. Aiyer, D. S. Chauhan, R. Srivastava and K. Selvaraj, *Nanoscale*, 2016, **8**, 4537–4546.

7   A. Agostini, L. Mondragón, C. Coll, E. Aznar, M. D. Marcos, R. Martínez-Máñez, F. Sancenón, J. Soto, E. Pérez-Payá and P. Amorós, *ChemistryOpen*, 2012, **1**, 17–20.

8   A. García-Fernández, G. García-Laínez, M. L. Ferrándiz, E. Aznar, F. Sancenón, M. J. Alcaraz, J. R. Murguía, M. D. Marcos, R. Martínez-Máñez, A. M. Costero and M. Orzáez, *J. Control. Release*, 2017, **248**, 60–70.

9   A. Ultimo, C. Giménez, P. Bartovsky, E. Aznar, F. Sancenón, M. D. Marcos, P. Amorós, A. R. Bernardo, R. Martínez-Máñez, A. M. Jiménez-Lara and J. R. Murguía, *Chem. - A Eur. J.*, 2016, **22**, 1582–1586.

10 L. Polo, N. Gómez-Cerezo, E. Aznar, J.-L. Vivancos, F. Sancenón, D. Arcos, M. Vallet-Regí and R. Martínez-Máñez, *Acta Biomater.*, 2017, **50**, 114–126.

11 Z. Luo, X. Ding, Y. Hu, S. Wu, Y. Xiang, Y. Zeng, B. Zhang, H.

Yan, H. Zhang, L. Zhu, J. Liu, J. Li, K. Cai and Y. Zhao, *ACS Nano*, 2013, **7**, 10271–10284.

12   Q. Zhang, K. Gee Neoh, L. Xu, S. Lu, E. Tang Kang, R. Mahendran and E. Chiong, *Langmuir*, 2014, **30**, 6151–6161.

13   R. Guillet-Nicolas, A. Popat, J.-L. Bridot, G. Monteith, S. Z. Qiao and F. Kleitz, *Angew. Chemie Int. Ed.*, 2013, **52**, 2318–2322.

14   E. Bringas, Ö. Köysüren, D. V. Quach, M. Mahmoudi, E. Aznar, J. D. Roehling, M. D. Marcos, R. Martínez-Máñez, P. Stroeve and D. S. Kohane, *Chem. Commun.*, 2012, **48**, 5647–5649.

15   M. Oroval, E. Climent, C. Coll, R. Eritja, A. Aviñó, M. D. Marcos, F. Sancenón, R. Martínez-Máñez and P. Amorós, *Chem. Commun.*, 2013, **49**, 5480–5482.

16   D. He, X. He, K. Wang, M. Chen, Y. Zhao, Z. Zou, J. Shi, Y. Kondo, R. Sawa, T. Fujimoto, T. Machinami and A. Ono, *J. Mater. Chem. B*, 2013, **1**, 1552–1560.

17   L. Chen, X. Zhou, W. Nie, Q. Zhang, W. Wang, Y. Zhang and C. He, *ACS Appl. Mater. Interfaces*, 2016, **8**, 33829–33841.

18   J. G. Croissant, D. Zhang, S. Alsaiari, J. Lu, L. Deng, F. Tamanoi, A. M. AlMalik, J. I. Zink and N. M. Khashab, *J. Control. Release*, 2016, **229**, 183–191.

19   M. Oroval, P. Díez, E. Aznar, C. Coll, M. D. Marcos, F. Sancenón, R. Villalonga and R. Martínez-Máñez, *Chem. - A Eur. J.*, 2017, **23**, 1353–1360.

20   C. Chen, J. Geng, F. Pu, X. Yang, J. Ren and X. Qu, *Angew. Chemie - Int. Ed.*, 2011, **50**, 882–886.

21   X. Yang, X. Liu, Z. Liu, F. Pu, J. Ren and X. Qu, *Adv. Mater.*, 2012, **24**, 2890–2895.

22   Z. Deng, Z. Zhen, X. Hu, S. Wu, Z. Xu and P. K. Chu, *Biomaterials*, 2011, **32**, 4976–4986.

23   L. Palanikumar, E. S. Choi, J. Y. Cheon, S. H. Joo and J.-H. Ryu, *Adv. Funct. Mater.*, 2015, **25**, 957–965.

24   L.-L. Li, M. Xie, J. Wang, X. Li, C. Wang, Q. Yuan, D.-W. Pang, Y. Lu and W. Tan, *Chem. Commun.*, 2013, **49**, 5823–5825.

25   I. Häuselmann and L. Borsig, *Front. Oncol.*, 2014, **4**, 28.

26   J. B. Haltiwanger, R. S. & Lowe, *Annu. Rev. Biochem.*, 2004, **73**, 491–537.

27   A. Varki, R. Kannagi and B. P. Toole, *Glycosylation Changes in Cancer*, Cold Spring Harbor Laboratory Press, 2009.

28   A. Varki and J. B. Lowe, *Biological Roles of Glycans*, Cold Spring Harbor Laboratory Press, 2009.

29   M. Gary-Bobo, O. Hocine, D. Brevet, M. Maynadier, L. Raehm, S. Richeter, V. Charasson, B. Loock, A. Morère, P. Maillard, M. Garcia and J. O. Durand, *Int. J. Pharm.*, 2012, **423**, 509–515.

30   D. Brevet, M. Gary-Bobo, L. Raehm, S. Richeter, O. Hocine, K. Amro, B. Loock, P. Couleaud, C. Frochot, A. Morère, P. Maillard, M. Garcia and J.-O. Durand, *Chem. Commun. (Camb).*, 2009, **28**, 1475–1477.

31   O. Hocine, M. Gary-Bobo, D. Brevet, M. Maynadier, S. Fontanel, L. Raehm, S. Richeter, B. Loock, P. Couleaud, C. Frochot, C. Charnay, G. Derrien, M. Smaïhi, A. Sahmoune, A. Morère, P. Maillard, M. Garcia and J. O. Durand, *Int. J. Pharm.*, 2010, **402**, 221–230.

32   I. Y. Park, I. Y. Kim, M. K. Yoo, Y. J. Choi, M. H. Cho and C. S. Cho, *Int. J. Pharm.*, 2008, **359**, 280–287.

33   Z. Luo, K. Cai, Y. Hu, L. Zhao, P. Liu, L. Duan and W. Yang, *Angew. Chemie - Int. Ed.*, 2011, **50**, 640–643.

34   J. Peng, K. Wang, W. Tan, X. He, C. He, P. Wu and F. Liu, *Talanta*, 2007, **71**, 833–840.

35   M. Yu, S. Jambhrunkar, P. Thorn, J. Chen, W. Gu and C. Yu, *Nanoscale*, 2013, **5**, 178–183.

36   Q. He, M. Ma, C. Wei and J. Shi, *Biomaterials*, 2012, **33**, 4392–4402.

37   S. Wu, X. Huang and X. Du, *Angew. Chemie Int. Ed.*, 2013, **52**, 5580–5584.

38   J. Li, X. Qu, G. F. Payne, C. Zhang, Y. Zhang, J. Li, J. Ren, H. Hong and C. Liu, *Adv. Funct. Mater.*, 2015, **25**, 1404–1417.

39   J. Burchell, R. Poulsom, A. Hanby, C. Whitehouse, L. Cooper, H. Clausen, D. Miles and J. Taylor-Papadimitriou, *Glycobiology*, 1999, **9**, 1307–1311.

40   S. S. Pinho, C. A. Reis, J. Paredes, A. M. Magalhães, A. C. Ferreira, J. Figueiredo, W. Xiaogang, F. Carneiro, F. Gärtner and R. Seruca, *Hum. Mol. Genet.*, 2009, **18**, 2599–2608.

41   M. Takahashi, M. Kuroki, K. Ohtsubo and N. Taniguchi, *Carbohydr. Res.*, 2009, **344**, 1387–1390.

42   M. Li, L. Song and X. Qin, *J. Biosci.*, 2010, **35**, 665–673.

43   K. Nagao, Y. Itoh, K. Fujita and M. Fujime, *Int. J. Urol.*, 2007, **14**, 795–799.

44   W. Gao, J. Liang and Y. Liang, *Onco. Targets. Ther.*, 2016, **9**, 3113–3125.

45   P. Sozzani, R. Arisio, M. Porpiglia and C. Benedetto, *Int. J. Surg. Pathol.*, 2008, **16**, 365–374.

46   A. Yusa, K. Miyazaki, N. Kimura, M. Izawa and R. Kannagi, *Cancer Res.*, 2010, **70**, 4064–4073.

47   A. Takada, K. Ohmori, T. Yoneda, K. Tsuyuoka, A. Hasegawa, M. Kiso and R. Kannagi, *Cancer Res.*, 1993, **53**, 354–361.

48   D. Golijanin, Y. Sherman, A. Shapiro and D. Pode, *Urology*, 1995, **46**, 173–177.

49   A. Hittelet, I. Camby, N. Nagy, H. Legendre, Y. Bronckart, C. Decaestecker, H. Kaltner, N. E. Nifant'ev, N. V Bovin, J. Pector, I. Salmon, H. Gabius, R. Kiss and P. Yeaton, *Lab. Invest.*, 2003, **83**, 777–787.

50   C. de la Torre, I. Casanova, G. Acosta, C. Coll, M. J. Moreno, F. Albericio, E. Aznar, R. Mangues, M. Royo, F. Sancenón and R. Martínez-Máñez, *Adv. Funct. Mater.*, 2015, **25**, 687–695.

51   J. M. De la Fuente and S. Penadés, *Tetrahedron Asymmetry*, 2002, **13**, 1879–1888.

52   T. Zhu and G.-J. Boons, *J. Am. Chem. Soc.*, 2000, **122**, 10222–10223.

53   O. Martínez-Ávila, K. Hijazi, M. Marradi, C. Clavel, C. Campion, C. Kelly and S. Penadés, *Chem. - A Eur. J.*, 2009, **15**, 9874–9888.

54   A. H. Cory, T. C. Owen, J. A. Barltrop and J. G. Cory, *Cancer Commun.*, 1991, **3**, 207–212.

55   G. Malich, B. Markovic and C. Winder, *Toxicology*, 1997, **124**, 179–192.

56   K. Sakuma, M. Aoki and R. Kannagi, *Proc. Natl. Acad. Sci. U. S. A.*, 2012, **109**, 7776–7781.